Chem

CellPress

Article

Self-assembled molecular-electronic films controlled by room temperature quantum interference

Marjan Famili[2,7], Chuancheng Jia[1,7], Xunshan Liu[3,7], Peiqi Wang[1,4], Iain M. Grace[2], Jian Guo[4], Yuan Liu[4,5], Ziying Feng[1], Yiliu Wang[1], Zipeng Zhao[4], Silvio Decurtins[3], Robert Häner[3], Yu Huang[4,6,*], Shi-Xia Liu[3,*], Colin J. Lambert[2,8,*] and Xiangfeng Duan[1,6,*]

[1]Department of Chemistry and Biochemistry, University of California, Los Angeles, Los Angeles, CA 90095, USA.
[2]Physics Department, Lancaster University, Lancaster LA1 4YB, UK.
[3]Department of Chemistry and Biochemistry, University of Bern, Freiestrasse 3, CH-3012 Bern, Switzerland.
[4]Department of Materials Science and Engineering, University of California, Los Angeles, California 90095, USA
[5]Key Laboratory for Micro-Nano Optoelectronic Devices of Ministry of Education, School of Physics and Electronics, Hunan University, Changsha 410082, China
[6]California NanoSystems Institute, University of California, Los Angeles, Los Angeles, CA 90095, USA.
[7]These authors contributed equally
*Correspondence: xduan@chem.ucla.edu (X.D.), c.lambert@lancaster.ac.uk (C.J.L.), liu@dcb.unibe.ch (S-X.L.), yhuang@seas.ucla.edu (Y.H.)
[8]Lead Contact: c.lambert@lancaster.ac.uk

SUMMARY

If single-molecule, room-temperature, quantum interference (QI) effects could be translated into massively parallel arrays of molecules located between planar electrodes, QI-controlled molecular transistors would become available as building blocks for future electronic devices. Here, we demonstrate unequivocal signatures of room-temperature QI in vertical tunnelling transistors, formed from self-assembled monolayers (SAMs), with stable room-temperature switching operations. Due to constructive QI effects, the conductances of the junctions formed from anthanthrene-based molecules with two different connectivities differ by a factor of 34, which can further increase to 173 by controlling the molecule-electrode interface with different terminal groups. Field-effect control is achieved using an ionic liquid gate, whose strong vertical electric field penetrates through the graphene layer and tunes the energy levels of the SAMs. The resulting room-temperature on-off current ratio of the lowest-conductance SAMs can reach up to 306, about one order of magnitude higher than that of the highest-conductance SAMs.

Keywords: Molecular junctions • Quantum interference • Transistor• Self-assembled monolayer

INTRODUCTION

Molecular electronics represent an attractive alternative for future electronic devices with potential to deliver logic gates, sensors, memories and thermoelectric energy harvesters with ultra-low power requirements and sub-10 nm device footprints.[1-4] Single-molecule electronic junctions have been investigated intensively over the past decade, not only as stepping stones towards functional devices/circuits made from collections of molecules, but also because their room-temperature electrical conductance is controlled by quantum interference (QI).[5-15] Figure 1A illustrates an example of a non-classical QI effect, in a graphene-like (anthanthrene) molecular core, when electrical current is injected and collected via the green arrows, or alternatively via the red arrows. If the core behaved like a classical resistor network, then the electrical conductance for these two connectivities would be approximately equal. In contrast, theory predicts and experiment confirms[16-18] that the room temperature, single-molecule, low-bias electrical conductance G_1 for the green (7,2') connectivity is approximately two orders of magnitude larger than the conductance G_2 of the red (1,5') connectivity. This is a clear signature of their different degrees of constructive QI

(Figure S5). The chemical realization of the green connectivity is molecule **1** of Figure 1B, in which the terminal groups attached to electrodes inject a current into the anthanthrene core via triple bonds **(Supplemental scheme 1)**. Similarly, molecules **2** and **3** are realisations of the red connectivity, with different terminal groups, which can further control the interfacial coupling and energy level alignment between the molecule and electrode[19,20]. Our aim is to create a SAM-based molecular tunnelling transistor from these molecules and to demonstrate that these single-molecule signatures of QI can be realised in self-assembled monolayer-based devices. We indeed find that the electrical conductance of the SAM formed from **1** is significantly higher than that of the SAM formed from **2** or **3**. Furthermore, by applying an external gate, we are able to assess their different field-effect performances.

RESULTS

Construction of the devices

In contrast to molecular tunnelling transistors fabricated by placing a solid back gate[21] or electrochemical gate[22,23] to the side of molecular junctions, which can typically only operate stably at cryogenic temperatures, here we utilise a vertical molecular tunnelling transistor with stable room-temperature operation, based on a gate modulated graphene/SAM/gold cross-plane vertical heterostructure.[24,25] The binding geometry of the molecules in the SAM are fixed[26] by the terminal anchor groups to the gold electrode and the inter molecular interactions in the SAM, which promote stable charge transport through the molecular junctions. A strong gating electric field, generated from the electrical double layer (EDL) of ionic liquid,[27] is vertically applied to the graphene/SAM/gold junctions (Figure 2A). Due to the partial electrostatic transparency of graphene,[28] the applied electric field penetrates through the graphene layer and tunes the energy levels of the SAM relative to the Fermi energy of gold (E_F^{gold}), resulting in effective gate control and a significant conductance modulation in the molecular transistors.

The fabrication processes for the vertical molecular tunnel transistors are shown schematically in the Supplemental information Figure S1. Figures 2B,C show a schematic illustration of the structure and an optical photograph of the fabricated device. An ultra-flat Au film is deposited on the exposed conducting silicon surface in a small hole at the centre of a silicon/SiO_2 chip, which is connected to a metal electrode at the corner and used as the source electrode. A self-assembled monolayer of molecule **1**, **2** or **3** (Figure 1B) is then functionalized on the Au film, and confirmed by atomic force microscopy (AFM), X-ray photoelectron spectroscopy (XPS) and Raman characterization (Figures S2–4). Chemical vapor deposition (CVD) grown single- layer graphene (SLG)[29] (Figure S4A) is then transferred and patterned on the top of the SAM. A drain electrode connecting with the graphene sheet and gate electrode is laid around the functional centre. Finally, a small amount of diethylmethyl(2-methoxyethyl)ammonium bis(trifluoromethylsulfonyl)imide (DEME-TFSI) ionic liquid is dropped on the graphene/SAM/gold channel and gate electrode. Since the binding geometry and conformation of the molecules are fixed in SAMs[26] and graphene electrodes prevent direct contact between the SAM and ionic liquid, stable devices can be realized with low noise operation at room temperature.

Charge transport in molecular junctions

In the absence of electrically active side chains, the ratio $\frac{G_1}{G_2}$ of the low-bias, single-molecule conductances of **1** and **2** are predicted by a 'magic number' table provided in reference[16], which yields $\frac{G_1}{G_2} = 81$ (Figure S5). This simple 'magic ratio theory' illustrates how connectivity alone contributes to conductance ratios, without including chemical effects or coulomb interactions. When the latter are included, recent studies indicate that the qualitative trend in the ratio is preserved (*i.e.*, that $\frac{G_1}{G_2} \gg 1$), but the precise value should be calculated using ab initio methods.

Figure 3B shows the computed transmission coefficient for electrons passing through all three junctions. Previous comparison between experiment and theory revealed that electron transport through single anthanthrene-based molecules attached to gold electrodes takes place near the middle of the energy gap between the highest occupied molecular orbital (HOMO) and the lowest unoccupied molecular orbital (LUMO).[16] Therefore in the

calculations presented below, the Fermi energy of the gold is located near the middle of the HOMO-LUMO gap and all energy axes are plotted with respect to the mid-gap energy $E_F^{mid-Gap} = E_F^{Gold}$. The computed ratio of their transmission coefficients in graphene-molecule-gold junctions (Figure S7A) for molecule **2** and **1** at $E = E_F^{Gold}$ is 116. It should be emphasised that both molecules exhibit constructive QI near their gap centres and the conductance ratio arises from the different degrees of constructive QI associated with the different connectivities. Figure S6 illustrates that the constructive nature of the QI is also reflected in the molecular orbitals of molecule **2** and **1**. When the terminal groups of molecules are changed from thiol to pyridine, the transmission coefficient in the junctions for molecule **3** at $E = E_F^{Gold}$ is reduced to 1/7 of that for molecule **2**. This indicates that the QI effect acts in conjunction with the higher pyridine-gold interface resistance[30] to determine charge transport in the junctions.

The experimental current density (J_D) *vs.* bias voltage (V_D) and the differential conductance (d*J*/d*V*) *vs.* V_D are shown in Figures 3C,D. As predicted by magic ratio theory, the current density (J_D) and for the 1,5' junction formed from molecule **2** is considerably lower than that of the 7,2' junction formed from molecule **1**, especially near zero bias, which is consistent with the transmission coefficient characteristics of the respective molecules discussed above and theoretical results (Figure 3E). With pyridine terminal groups for the 1,5' junction, the J_D for molecule **3** is further reduced, in agreement with the transmission functions.

The minima in the d*J*/d*V* curves are associated with the Dirac point of the graphene and their position relative to the zero V_D indicates whether the graphene is p-doped or n-doped. In Figure 3D, the Dirac point for molecule **1** and **2** samples occurs at –0.03 V and –0.05 V respectively, indicating that the graphene is slightly n-doped in the presence of the thiol-terminated SAMs. However, for sample **3** this minimum appears at 0.01V, suggesting p-doped graphene in the case of a pyridine anchor group. For this reason, in what follows, when comparing our calculated *T*(*E*) with experiments, the band structure of the graphene is adjusted to place the Dirac point of each system at the experimental value.

For the experimental d*J*/d*V* results (Figure 3D), the value of d*J*/d*V* at zero bias for molecule **1** is 29 times larger than that of molecule **2**. From the statistics of 19 different experimental devices (Supplemental Information, Section S6), the zero-bias differential conductance for molecule **1** is 34 times larger than that for molecule **2** (Table S1). This ratio is comparable with the value of 84 obtained from the theoretical results of Figure 3F. It is also worth mentioning that for molecule **2** and **1** junctions with gold-molecule-gold contacts (Figure S8), the conductance ratio at zero bias is $\frac{G_1}{G_2} = 203$, which indicates that the interfacial contacts are playing a role in determining the conductance ratio. After changing the terminal groups from thiol to pyridine to control the interfacial contacts, the zero-bias differential conductance for molecule **3** is 1/5.0 of that for molecule **2**, which is 1/5.1 from statistics of 19 different experimental devices (Table S1). This value is also comparable with the calculated value of 1/8.7 (Figure 3F).

Field effect properties of the transistors

To probe the field effect performances of these molecular junctions, DEME-TFSI ionic liquid was used for gating, which has a large electrochemical window, a high ionic conductivity, and a low freezing temperature for ion migration.[31] When a gate voltage (V_G) is applied to the gate electrode, a Helmholtz electrical double layer (EDL) self-organizing on the outside surface of graphene layer (Figures 2A,B) generates a strong electric field up to ~ 10 MV/cm to the molecular junction.[27] The gate performances of three transistors were measured at room temperature (298 K). Figures 4A, 4D and 4G show typical gate dependent J_D-V_D characteristics for molecules **1, 2** and **3**, respectively. Changing V_G from –1 to 1 V, greatly increases J_D for negative V_D, while J_D greatly decreases with V_G for positive V_D, clearly demonstrating effective field-effect modulation of the molecular junctions (Supplemental Information, Section S7).

Typical gate dependent d*J*/d*V*-V_D characteristics for molecules **1, 2** and **3** are shown in Figures 4B,E,H. When the gate voltage is increased from –1 to 1 V, d*J*/d*V*-V_D curves for all three

junctions move in a positive direction along the V_D axis, which reflects the gate-voltage dependent movement of the molecular orbital energy levels. Figures 4C, 4F and 4I respectively show two-dimensional visualizations of d*I*/d*V* plotted versus V_G and V_D for molecules **1, 2** and **3**. The oblique diamond-shaped low conductance region (green and blue) can be observed for all three transistors, which indicate off-resonant transport through HOMO-LUMO gap. While, the red-orange high-conductance region outside the diamond is due to the conductive frontier molecular orbitals entering the bias window. The relative conductance change between center low conductance and outside high conductance regions for molecule **1** is considerably smaller than that for molecule **2**, which indicates the better gating tunability for molecule **1**. This agrees with the calculated *T*(*E*) for molecules **1** and **2** (Figure 3B), as the difference between off-resonant and resonant transport is more pronounced for molecule **2** in comparison with molecule **1**. For comparison between molecules **3** and **2**, a blue lowest conductance region appears at the center of the diamond for molecule **3** (Figure 4F), corresponding to the calculated lowest off-resonant transmission of **3** (Figure 3B), which further improves the gating tunability of molecule **3**.

The conductance minima for molecule **1** are sharp features for all values of the applied gate voltage. However, in the case of molecule **2** (Figure 4E) the minimum at $V_G = 0$ V is a broader feature, which splits into two sharper minima when the gate voltage is increased to 0.5 V and 1.0 V. (For examples of other devices see Supplemental figures S10-S27.) This is in agreement with the calculated *T*(*E*) for molecules **1** and **2** (Figure 3B). While T_1 has no features between the HOMO and LUMO apart from the Dirac point, T_2 has two sharp anti-resonances. For $V_G = 0$ none of the anti-resonances are close enough to the Fermi energy to appear in the d*I*/d*V* curves. By increasing the gate voltage, and hence the relative position of the anti-resonances to the Fermi energy, one of the anti-resonances is close enough to the Fermi-energy to be captured in the d*I*/d*V*. The lever arms in the theoretical model (see theoretical methods), which give the best agreement between theory and experiment, are $\alpha = 0.4$, $\gamma = 0.25$ and $\beta = 0.25$.

Working mechanism of the transistors

Figures 5A, 5D and 5G show the V_D dependence of *T*(*E*) versus $E - E_F^{Gold}$ for molecules **1**, **2** and **3**. It is assumed that the energies of the molecular levels relative to E_F^{Gold} are independent of V_D and that positive (negative) bias voltage decreases (increases) the Dirac point relative to E_F^{Gold} (Eq. 1 in supplemental computational methods). The current is computed using Eq. 4 (see supplemental computational methods) by evaluating individual transmission coefficients *T*(*E*, V_D, V_G) at every V_D value and computing the associated current. The d*I*/d*V* curves are then obtained by differentiating the current with respect to V_D.

The V_D and V_G dependent transmission coefficient *T*(*E*, V_D, V_G) was calculated using the quantum transport code Gollum[32] and the current obtained from Eq. 4 (see supplemental computational methods). The theoretical gate-dependent I_D-V_D characteristics for molecule **2** (Figure 5E) reveal that when V_G changes from -0.6 to 0.6 V, I_D greatly increases with V_G for negative V_D, while I_D decreases with V_G for positive V_D. A similar theoretical gate dependent I_D-V_D characteristic is also obtained for molecule **1** (Figure 5B), though the gate dependent change in I_D is smaller than that for molecule **2**. Furthermore, from the gate dependent d*I*/d*V*-V_D characteristics for molecule **2** (Figure 5F), it can be observed that the d*I*/d*V*-V_D curve shifts in a positive direction with V_G changing from -0.6 to 0.6 V, especially for the lowest conductance points. For molecule **1**, a similar gate dependent d*I*/d*V*-V_D curve is obtained, but with relatively smaller amplitude (Figure 5C), in qualitative agreement with the experimental results (Figure 4). For molecule **3**, gate dependent I_D-V_D (Figure 5H) and d*I*/d*V*-V_D (Figure 5I) curve with relatively larger amplitude can be observed, which are similar to molecule **2**. Moreover, the lowest conductance minima appear in gate dependent d*I*/d*V*-V_D curves (Figure 5I), which is consistent with the experimental lowest conductance region (Figure 4I).

Transfer characteristics of the transistors

Transfer characteristics, monitoring the current modulation with varying V_G at a fixed V_D, are widely used for assessing transistor performance[33]. The V_D dependent transfer characteristics for molecules **1**, **2** and **3** were investigated by both experimentally and theoretically. Experimental transfer characteristics (J_D-V_G) for **1** at V_D = –0.1, –0.2, –0.4, –0.6 and –0.8 V are shown in Figure 6A. (For further devices see Figs S28-S33.) It can be observed that the lowest current point at V_D = –0.1 V is near V_G = 0 V; and with V_D changing from –0.1 to –0.8 V, the lowest current point shifts to more negative V_D. As the Dirac point of the graphene electrode dominates the conductance minima for molecule **1** (Figure 5A), such shifting of the lowest current point is due to the variation of the Dirac point of the graphene electrode. Specifically, with more negative V_D, an increased negative V_G is needed to move the central transmission dip of the junction to the middle of the bias window. This experimental phenomenon is also confirmed by the theoretical transfer characteristics (I_D-V_G) for **1** (Figure 6D), as V_D changes from –0.1 to –0.8 V. Similar behaviour occurs for J_D-V_G curves with positive V_D (Figure S28A). The on-off ratio, which corresponds to the ratio between the highest and lowest currents in a J_D-V_G curve, is up to 26 for molecule **1** near V_D = 0 V (Figure S28B). In contrast, the highest on-off ratio for molecule **2** (Figure 6B) is increased to 105 near V_D = 0 V (Figure S28D), which is about 4 times of molecule **1**. Furthermore, two conductance valleys can be obviously observed from J_D-V_G curves, especially at V_D = –0.1 V, which is due to the QI-induced conductance minima for molecule **2**. This is clear from the theoretical transfer characteristics (I_D-V_G) of molecule **2** (Figure 6E), where two conductance valleys appear and become mixed together with V_D changing from –0.1 to –0.8 V. Furthermore, the on-off ratio decreases with increasing $|V_D|$, which can be attributed to electron transmission occurring over a wider bias window, with the conductance being less sensitive to gating-induced movement of molecular energy levels. Similar transfer characteristics appear for molecule **3** (Figure 6C), and the highest on-off ratio is further increased to 306 near V_D = 0 V (Figure S28F), which is about 2.9 times of molecule **2** and 12.0 times of **1**. This is consistent with the theoretical transfer characteristics (I_D-V_G) for **3** (Figure 6C), because two conductance valleys appear, and on-off ratios decrease as V_D changes from –0.1 to –0.8 V.

DISCUSSION

In summary, we have demonstrated that unequivocal signatures of single-molecule room-temperature QI can be translated into self-assembled molecular films. Furthermore anthanthrene-based molecular transistors, formed from vertical cross-plane graphene/SAM/gold heterostructures and ionic liquid gating, are shown to exhibit stable room-temperature switching operations. With two different connectivities to the anthanthrene core, QI effects lead to a conductances ratio of approximately 34 for molecular junctions **1** and **2**, which can be further enlarged to 173 for junction **3** by controlling the molecule-electrode interface with different terminal groups. It should be noted that all three studied molecules exhibit constructive QI. For graphene-like molecules, the term 'destructive QI' is conventionally applied to connectivities for which counting rules[34] identify a zero in the transmission coefficient near the middle of their HOMO-LUMO gap. Equivalently, this would mean that the corresponding magic number vanishes. For the two connectivities considered here, the magic numbers and mid-gap transmissions are non-zero, therefore the molecules with different connectivities exhibit different degrees of constructive QI. Importantly, junction **3** can show a significance current modulation by an ionic liquid gate, with a maximum on–off ratio up to 306, which is about one order of magnitude higher than that for **1**. This enhanced gate behaviour for **3** is a direct consequence of the zero-bias conductance suppression induced by QI, combined with a higher interfacial resistance. The designed QI-controlled molecular transistors with large on/off ratio are potential electronic building blocks for future integrated circuits and functional ultra-thin film materials. From the viewpoint of fundamental science, the advantage is that incorporating a molecular layer in a g-FET device enables this first demonstration that constructive QI effects are preserved in SAMs. This is significant, because it means that QI-based strategies for enhancing monolayer materials properties such as the electrical conductance, thermal conductance and Seebeck coefficient of SAMs can be pursued in the future with confidence. From a g-FET device viewpoint, QI-SAMs can improve intrinsic field-effect properties and expand other functionalities of the device.

EXPERIMENTAL PROCEDURES

Full experimental procedures are provided in the Supplemental Information.

SUPPLEMENTAL INFORMATION

Supplemental Information includes Supplemental Experimental Procedures, 33 figures, and 1 table and can be found with this article online at https://doi.org/10.1016/j.chempr.******.

ACKNOWLEDGMENTS

We acknowledge the Nanoelectronics Research Facility (NRF) at UCLA for technical support. X.D. acknowledges financial support by ONR through grant number N00014-15-1-2368. Support from the UK EPSRC is acknowledged, through grant nos. EP/N017188/1, EP/P027156/1 and EP/N03337X/1. Support from the European Commission is provided by the FET Open project 767187 – QuIET and the EU project BAC-TO-FUEL.

AUTHOR CONTRIBUTIONS

X.D., C.L. and C.J. conceived and designed the experiments. C.J. performed most of the experiments including device fabrication, characterization and data analysis. M.F. and I.G. performed the theoretical simulation and data analysis. X.L., S.D. and S-X.L. synthesized the molecules. P.W., J.G., Y.L. and Z.F. assisted with device fabrication and characterizations. Y.W. performed the AFM studies. Z.Z. performed the XPS studies. X.D., C.L., R.H., S-X.L. and Y.H. supervised the research. X.D., C.L., C.J., S-X.L. and M.F. co-wrote the paper. All authors discussed the results and commented on the manuscript.

DECLARATION OF INTERESTS

The authors declare no competing financial interests.

FIGURE TITLES AND LEGENDS

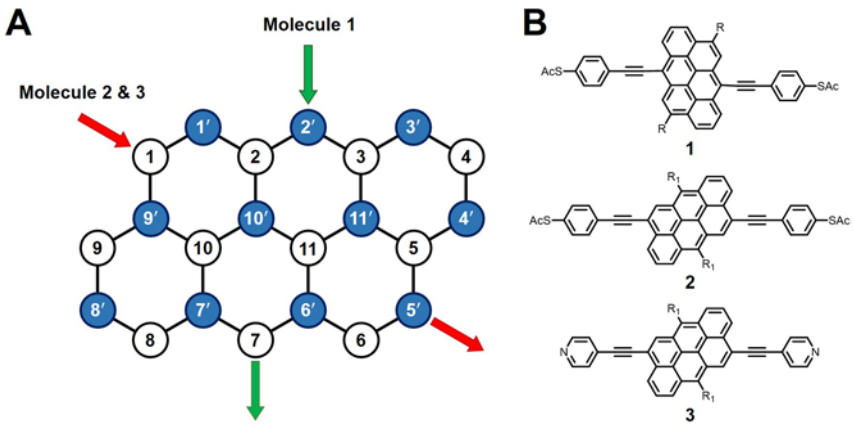

Figure 1. Structures of studied molecules

(A) A sketch of an anthanthrene core with connectivities 7,2' and 1,5'. (The numbering system is chosen for mathematical convenience and does not coincide with standard chemical notation.) (B) Chemical realisations of molecules with anthanthrene cores. **1** corresponds to the 7,2' connectivity, while **2** and **3** correspond to the 1,5' connectivity. R = 4-(2-ethylhexyloxy)phenyl, R_1 = -OC_8H_{17}.

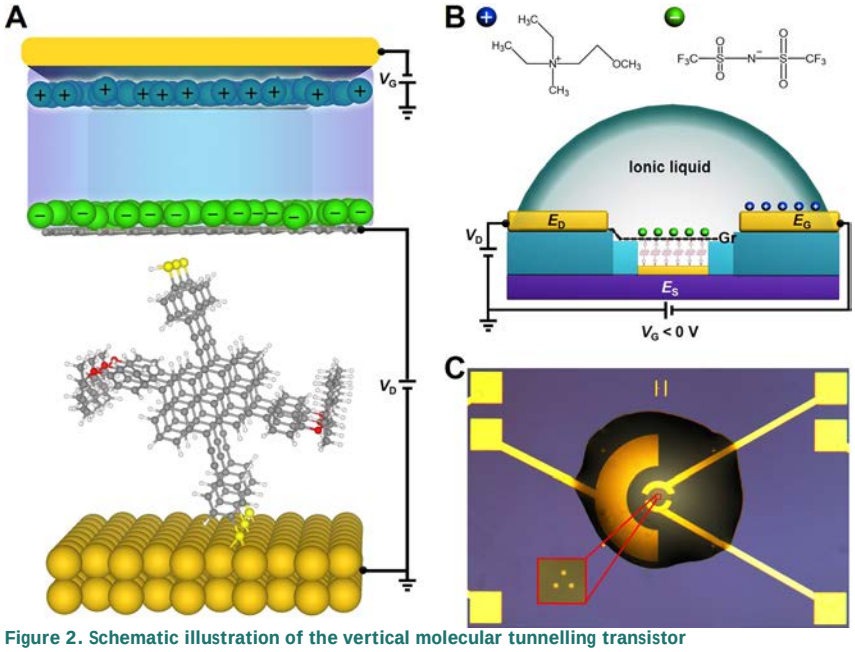

Figure 2. Schematic illustration of the vertical molecular tunnelling transistor

(A, B) Schematic illustration for the setup of the device with vertical ionic liquid gate through graphene layer to SAMs and molecular structures for $DEME^+$ cation and $TFSI^-$ anion. (C) Optical photograph of the device with ionic liquid gate.

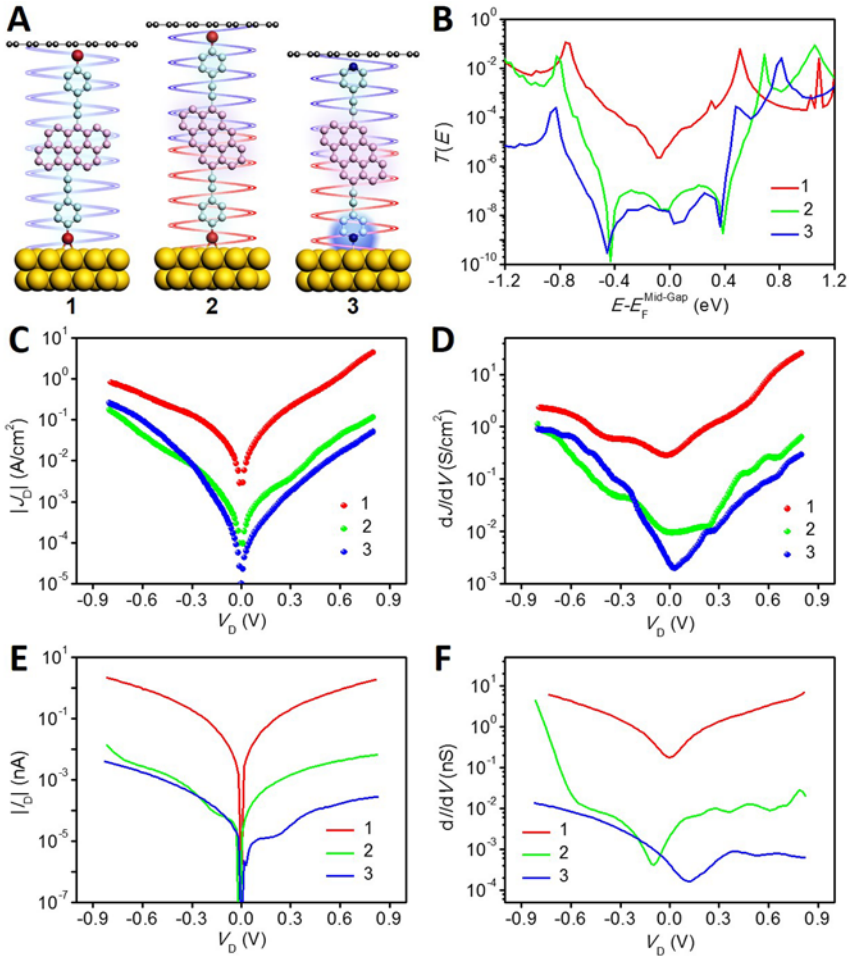

Figure 3. Charge transport in molecular junctions

(A) Schematic illustration of molecular junction **1**, **2** and **3**, where the side chains of molecules are hidden. (B) Transmission functions $T(E)$ for **1** (red), **2** (green) and **3** (blue). (C) Plots of experimental current density (J_D) *vs.* bias voltage (V_D) for **1**, **2** and **3**. (D) Experimental differential conductance (dJ/dV) *vs.* V_D. (E) Theoretical current (I_D) *vs.* V_D. (F) Theoretical differential conductance (dI/dV) *vs.* V_D.

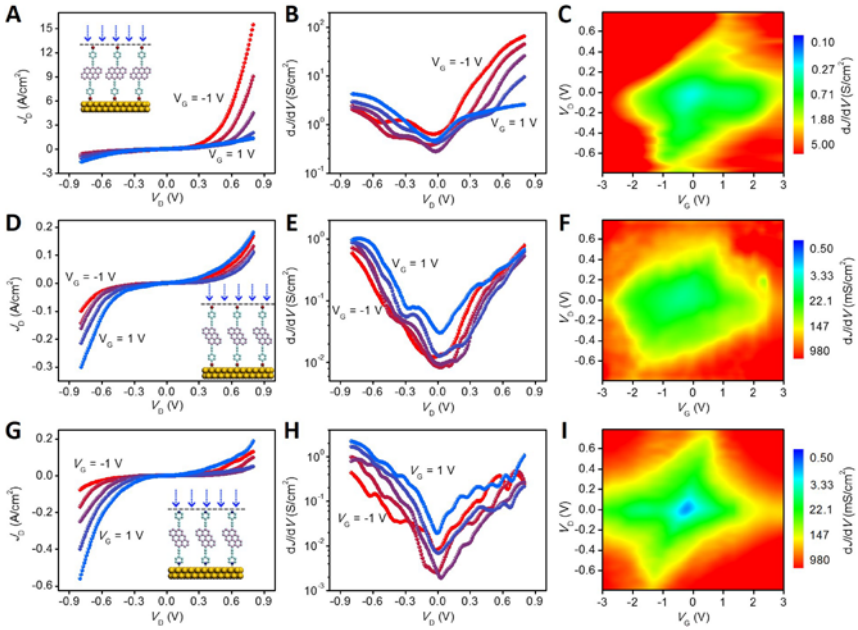

Figure 4. Gating charge transport in molecular transistors

(A, D, G) J_D *vs.* V_D characteristics for **1** (A), **2** (D), and **3** (G) with gate voltage (V_G) changing from –1 to 1 V with step of 0.5 V. Insets show schematics of the **1, 2** and **3** transistors with applied vertical electric field. (B, E, H) dJ/dV *vs.* V_D characteristics for **1** (B), **2** (E), and **3** (H) with V_G changing from –1 to 1 V with step of 0.5 V. (C, F, I) Two-dimensional visualization of dJ/dV *vs.* V_G and V_D for **1** (C), **2** (F), and **3** (I).

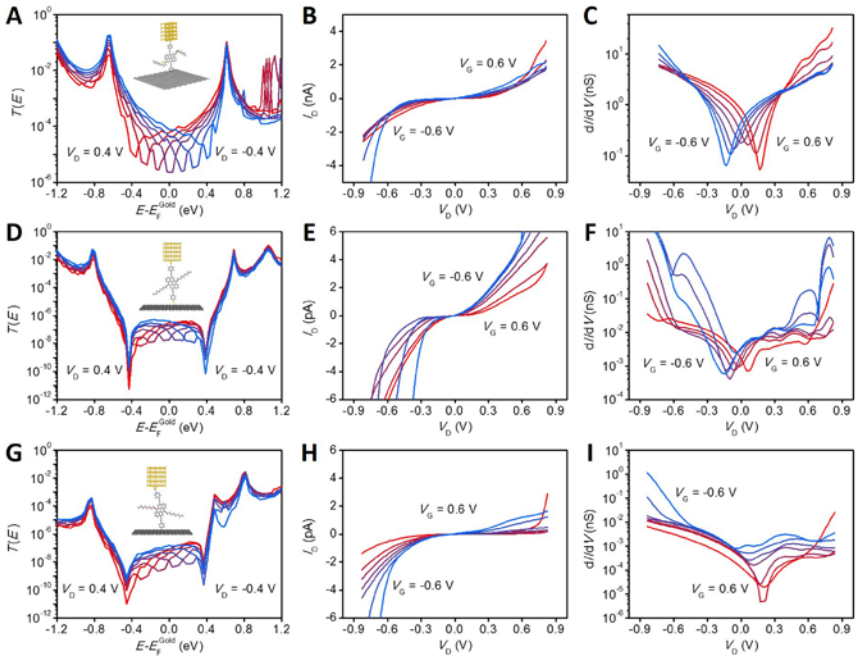

Figure 5. Working mechanism for vertical molecular transistors

(A, D, G) Transmission coefficient T(E) *vs.* $E - E_F^{Gold}$ for molecular junction **1** (A), **2** (D) and **3** (G) for $-0.4 < V_D < 0.4$ with steps of 0.13 V (red for V_D = 0.4 V). Insets show the structures of molecular junctions for simulation. (B, E, H) Gate dependent theoretical I_D-V_D characteristics for **1** (B), **2** (E) and **3** (H) for $-0.6 < V_G < 0.6$ with steps of 0.2 V (red for V_G = 0.6 V). (C, F, I) Gate dependent theoretical dI/dV-V_D characteristics for **1** (C), **2** (F) and **3** (I) for $-0.6 < V_G < 0.6$ with steps of 0.2 V (red for V_G = 0.6 V).

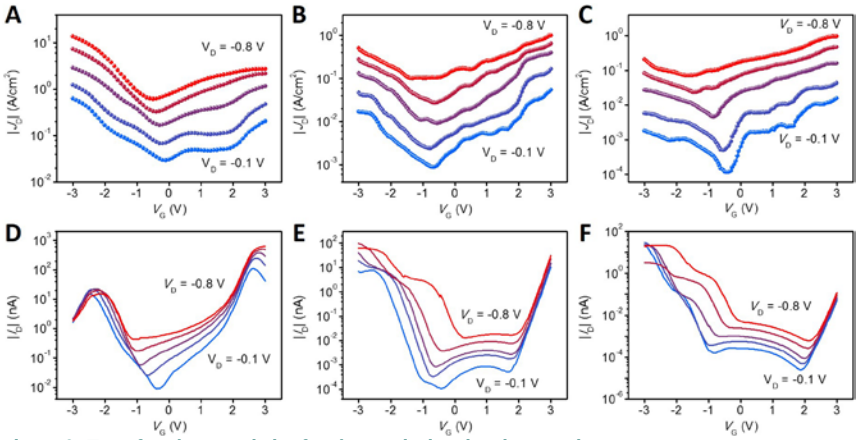

Figure 6. Transfer characteristics for the vertical molecular transistors

(A-C) Experimental transfer characteristics for **1** (A), **2** (B) and **3** (C). (D-F) Theoretical transfer characteristics for **1** (D)**, 2** (E) and **3** (F). V_D is varied from –0.1, –0.2, –0.4, –0.6 to –0.8 V in (A-F).

REFERENCES AND NOTES

1. Aradhya, S.V., and Venkataraman, L. (2013). Single-molecule junctions beyond electronic transport. Nat. Nanotech. *8*, 399–410.
2. Lambert, C. (2015). Basic concepts of quantum interference and electron transport in single-molecule electronics. Chem. Soc. Rev. *44*, 875–888.
3. Xiang, D., Wang, X., Jia, C., Lee, T., and Guo, X. (2016). Molecular-scale electronics: from concept to function. Chem. Rev. *116*, 4318–4440.
4. Jia, C., Migliore, A., Xin, N., Huang, S., Wang, J., Yang, Q., Wang, S., Chen, H., Wang, D., Feng, B., *et al.* (2016). Covalently bonded single-molecule junctions with stable and reversible photoswitched conductivity. Science *352*, 1443–1445.
5. Magoga, M., and Joachim, C. (1999). Conductance of molecular wires connected or bonded in parallel. Phys. Rev. B *59*, 16011.
6. Papadopoulos, T., Grace, I., and Lambert, C. (2006). Control of electron transport through Fano resonances in molecular wires. Phys. Rev. B *74*, 193306.
7. Markussen, T., Schiotz, J., and Thygesen, K.S. (2010). Electrochemical control of quantum interference in anthraquinone-based molecular switches. J. Chem. Phys. *132*, 224104.
8. Vazquez, H., Skouta, R., Schneebeli, S., Kamenetska, M., Breslow, R., Venkataraman, L., and Hybertsen, M. (2012). Probing the conductance superposition law in single-molecule circuits with parallel paths. Nat. Nanotech. *7*, 663–667.
9. Ballmann, S., Hartle, R., Coto, P.B., Elbing, M., Mayor, M., Bryce, M.R., Thoss, M., and Weber, H.B. (2012). Experimental evidence for quantum interference and vibrationally induced decoherence in single-molecule junctions. Phys. Rev. Lett. *109*, 056801.
10. Aradhya, S.V., Meisner, J.S., Krikorian, M., Ahn, S., Parameswaran, R., Steigerwald, M.L., Nuckolls, C., and Venkataraman, L. (2012). Dissecting contact mechanics from quantum interference in single-molecule junctions of stilbene derivatives. Nano Lett. *12*, 1643–1647.
11. Kaliginedi, V., Moreno-Garcia, P., Valkenier, H., Hong, W., Garcia-Suarez, V.M., Buiter, P., Otten, J.L., Hummelen, J.C., Lambert, C.J., and Wandlowski, T. (2012). Correlations between molecular structure and single-junction conductance: a case study with oligo(phenylene-ethynylene)-type wires. J. Am. Chem. Soc. *134*, 5262–5275.
12. Arroyo, C.R., Tarkuc, S., Frisenda, R., Seldenthuis, J.S., Woerde, C.H., Eelkema, R., Grozema, F.C., and van der Zant, H.S. (2013). Signatures of quantum interference effects on charge transport through a single benzene ring. Angew. Chem. *125*,, 3234–3237.
13. Guédon, C.M., Valkenier, H., Markussen, T., Thygesen, K.S., Hummelen, J.C., and Van Der Molen, S.J. (2012). Observation of quantum interference in molecular charge transport. Nat. Nanotech. *7*, 305–309.
14. Ke, S.-H., Yang, W., and Baranger, H.U. (2008). Quantum-interference-controlled molecular electronics. Nano Lett. *8*, 3257–3261.
15. Zhang, Y., Ye, G., Soni, S., Qiu, X., Krijger, T.L., Jonkman, H.T., Carlotti, M., Sauter, E., Zharnikov, M., and Chiechi, R.C. (2018). Controlling destructive quantum interference in tunneling junctions comprising self-assembled monolayers via bond topology and functional groups. Chemical science *9*, 4414-4423.
16. Geng, Y., Sangtarash, S., Huang, C., Sadeghi, H., Fu, Y., Hong, W., Wandlowski, T., Decurtins, S., Lambert, C.J., and Liu, S.X. (2015). Magic ratios for connectivity-driven electrical conductance of graphene-like molecules. J. Am. Chem. Soc. *137*, 4469–4476.
17. Sangtarash, S., Huang, C., Sadeghi, H., Sorohhov, G., Hauser, J., Wandlowski, T., Hong, W., Decurtins, S., Liu, S.X., and Lambert, C.J. (2015). Searching the Hearts of Graphene-like Molecules for Simplicity, Sensitivity, and Logic. J. Am. Chem. Soc. *137*, 11425–11431.

18. Lambert, C.J., and Liu, S.X. (2018). A Magic Ratio Rule for Beginners: A Chemist's Guide to Quantum Interference in Molecules. Chem. Eur. J. *24*, 4193–4201.
19. Jia, C., and Guo, X. (2013). Molecule-electrode interfaces in molecular electronic devices. Chem. Soc. Rev. *42*, 5642–5660.
20. Hong, W., Manrique, D.Z., Moreno-Garcia, P., Gulcur, M., Mishchenko, A., Lambert, C.J., Bryce, M.R., and Wandlowski, T. (2012). Single molecular conductance of tolanes: experimental and theoretical study on the junction evolution dependent on the anchoring group. J. Am. Chem. Soc. *134*, 2292–2304.
21. Moth-Poulsen, K., and Bjørnholm, T. (2009). Molecular electronics with single molecules in solid-state devices. Nat. Nanotech. *4*, 551–556.
22. Huang, C., Rudnev, A.V., Hong, W., and Wandlowski, T. (2015). Break junction under electrochemical gating: testbed for single-molecule electronics. Chem. Soc. Rev. *44*, 889–901.
23. Li, Z., Li, H., Chen, S., Froehlich, T., Yi, C., Schonenberger, C., Calame, M., Decurtins, S., Liu, S.X., and Borguet, E. (2014). Regulating a benzodifuran single molecule redox switch via electrochemical gating and optimization of molecule/electrode coupling. J. Am. Chem. Soc. *136*, 8867–8870.
24. Liu, Y., Weiss, N.O., Duan, X., Cheng, H.-C., Huang, Y., and Duan, X. (2016). Van der Waals heterostructures and devices. Nat. Rev. Mater. *1*, 16042.
25. Novoselov, K.S., Mishchenko, A., Carvalho, A., and Castro Neto, A.H. (2016). 2D materials and van der Waals heterostructures. Science *353*, aac9439.
26. Love, J.C., Estroff, L.A., Kriebel, J.K., Nuzzo, R.G., and Whitesides, G.M. (2005). Self-assembled monolayers of thiolates on metals as a form of nanotechnology. Chem. Rev. *105*, 1103–1170.
27. Ueno, K., Nakamura, S., Shimotani, H., Yuan, H., Kimura, N., Nojima, T., Aoki, H., Iwasa, Y., and Kawasaki, M. (2011). Discovery of superconductivity in KTaO3 by electrostatic carrier doping. Nat. Nanotech. *6*, 408–412.
28. Tian, T., Rice, P., Santos, E.J., and Shih, C.J. (2016). Multiscale analysis for field-effect penetration through two-dimensional materials. Nano Lett. *16*, 5044–5052.
29. Jia, C., Jiang, J., Gan, L., and Guo, X. (2012). Direct optical characterization of graphene growth and domains on growth substrates. Sci. Rep. *2*, 707.
30. Obersteiner, V., Egger, D.A., and Zojer, E. (2015). Impact of Anchoring Groups on Ballistic Transport: Single Molecule vs Monolayer Junctions. J. Phys. Chem. C *119*, 21198–21208.
31. Sato, T., Masuda, G., and Takagi, K. (2004). Electrochemical properties of novel ionic liquids for electric double layer capacitor applications. Electrochim. Acta *49*, 3603–3611.
32. Ferrer, J., Lambert, C.J., García-Suárez, V.M., Manrique, D.Z., Visontai, D., Oroszlany, L., Rodríguez-Ferradás, R., Grace, I., Bailey, S.W.D., Gillemot, K., *et al.* (2014). GOLLUM: a next-generation simulation tool for electron, thermal and spin transport. New J. Phys. *16*, 093029.
33. Yu, W.J., Li, Z., Zhou, H., Chen, Y., Wang, Y., Huang, Y., and Duan, X. (2013). Vertically stacked multi-heterostructures of layered materials for logic transistors and complementary inverters. Nat. Mater. *12*, 246–252.
34. Markussen, T., Stadler, R., and Thygesen, K.S. (2010). The relation between structure and quantum interference in single molecule junctions. Nano Lett. *10*, 4260–4265.